Protein Engineering, Design & Selection, 2017, vol. 30 no. 4, pp. 333–345
doi: 10.1093/protein/gzx003
Advance Access Publication Date: 4 February 2017
Original Article

OXFORD

Original Article

Overcoming an optimization plateau in the directed evolution of highly efficient nerve agent bioscavengers

Moshe Goldsmith[1,*], Nidhi Aggarwal[2], Yacov Ashani[1,2], Halim Jubran[1], Per Jr. Greisen[3], Sergey Ovchinnikov[3], Haim Leader[4], David Baker[3], Joel L. Sussman[2], Adi Goldenzweig[1], Sarel J. Fleishman[1], and Dan S. Tawfik[1,*]

[1]Department of Biomolecular Sciences, Weizmann Institute of Science, 234 Herzel St, Rehovot 7610001, Israel, [2]Department of Structural Biology, Weizmann Institute of Science, 234 Herzel St, Rehovot 7610001, Israel, [3]Institute for Protein Design, Department of Biochemistry, University of Washington, Seattle, WA 98195, USA, and [4]Department of Materials and Interfaces, Weizmann Institute of Science, 234 Herzel St, Rehovot 761001, Israel

[*]To whom correspondence should be addressed. E-mail: moshe.goldsmith@weizmann.ac.il; dan.tawfik@weizmann.ac.il
Edited by Sir Alan Fersht

Received 14 November 2016; Revised 5 January 2017; Editorial Decision 9 January 2017; Accepted 10 January 2017

Abstract

Improving an enzyme's initially low catalytic efficiency with a new target substrate by an order of magnitude or two may require only a few rounds of mutagenesis and screening or selection. However, subsequent rounds of optimization tend to yield decreasing degrees of improvement (diminishing returns) eventually leading to an optimization plateau. We aimed to optimize the catalytic efficiency of bacterial phosphotriesterase (PTE) toward V-type nerve agents. Previously, we improved the catalytic efficiency of wild-type PTE toward the nerve agent VX by 500-fold, to a catalytic efficiency (k_{cat}/K_M) of $5 \times 10^6\ M^{-1}\ min^{-1}$. However, effective *in vivo* detoxification demands an enzyme with a catalytic efficiency of $>10^7\ M^{-1}\ min^{-1}$. Here, following eight additional rounds of directed evolution and the computational design of a stabilized variant, we evolved PTE variants that detoxify VX with a $k_{cat}/K_M \geq 5 \times 10^7\ M^{-1}\ min^{-1}$ and Russian VX (RVX) with a $k_{cat}/K_M \geq 10^7\ M^{-1}\ min^{-1}$. These final 10-fold improvements were the most time consuming and laborious, as most libraries yielded either minor or no improvements. Stabilizing the evolving enzyme, and avoiding tradeoffs in activity with different substrates, enabled us to obtain further improvements beyond the optimization plateau and evolve PTE variants that were overall improved by >5000-fold with VX and by >17 000-fold with RVX. The resulting variants also hydrolyze G-type nerve agents with high efficiency (GA, GB at $k_{cat}/K_M > 5 \times 10^7\ M^{-1}\ min^{-1}$) and can thus serve as candidates for broad-spectrum nerve-agent prophylaxis and post-exposure therapy using low enzyme doses.

Key words: computational design, enzyme engineering, phosphotriesterase, PROSS, protein stability

Introduction

Directed evolution and engineering methods are increasingly used to optimize enzyme stability and catalytic efficiency with non-cognate substrates for industrial, bioremediation, biosensing and medical applications. However, most studies report improvements of up to two orders of magnitude in catalytic efficiencies with their target substrates; examples reviewed in (Yang and Withers, 2009; Wijma and Janssen, 2013; Currin *et al.*, 2015). In relatively few cases,

improvements in catalytic efficiencies of three or more orders of magnitude have been described; for examples see (Khare *et al.*, 2012; Zheng *et al.*, 2014; Obexer *et al.*, 2016). The initial catalytic efficiencies of wild-type or computationally designed enzymes with their target substrates are often very low-k_{cat}/K_M < 600 M^{-1} min^{-1} (Fasan *et al.*, 2007; Althoff *et al.*, 2012; Rockah-Shmuel and Tawfik, 2012). Thus, practical applications may require enhancements of catalytic efficiencies by ≥4 orders of magnitude for evolved enzymes to gain the efficiency of even an 'average' natural enzyme (k_{cat}/K_M) ≈ 6×10^6 M^{-1} min^{-1} (Bar-Even *et al.*, 2011).

Directed enzyme evolution is often performed under the assumption that evolving enzymes follow a gradual and continuous path of improvement for the selected trait. However, a pattern of diminishing returns, whereby the degree of improvement decreases with each round of evolution, is commonly observed both in natural (MacLean *et al.*, 2010; Chou *et al.*, 2011) and laboratory evolution (Tokuriki *et al.*, 2012). Diminishing returns are most likely to be encountered when attempting to improve an enzyme by over 4 orders of magnitude. In such cases, an 'optimization plateau' is reached. When improvements plateau, it is, however, unclear whether further improvements could be attained with additional, new mutations (i.e. the trajectory is held at a local peak) or the maximal catalytic efficiency for this given evolutionary trajectory has been obtained (the 'fitness' peak for this particular trajectory has been reached). There is also no way of telling if there is a completely different trajectory leading from the same starting point to a much higher activity (a global peak). At present, the challenges of improving enzymes past their 'optimization plateau' have not been commonly addressed in published works.

We aimed to obtain variants of a bacterial phosphotriesterase (PTE) capable of hydrolyzing V-type nerve agents, which are highly toxic organophosphates (OPs) that act following inhalation or through skin absorption. Specifically, we wanted to develop highly efficient, catalytic, nerve agent bioscavengers that could serve as prophylactic antidotes or as post-exposure treatments of nerve agent intoxications, against which current countermeasures have limited efficacy (Bird *et al.*, 2010; Worek *et al.*, 2016). Nerve agents are racemic mixtures, in which the S_P isomer is typically 100–1000 times more toxic than the R_P isomer (Benschop and Dejong, 1988). Therefore, effective and symptom-free prophylactic protection from lethal nerve agent doses, using low enzyme doses (≤1 mg/kg body weight), requires the detoxifying enzymes to have catalytic efficiency (k_{cat}/K_M) values of ≥ 5×10^7 M^{-1} min^{-1} toward the more toxic S_P isomers of nerve agents (Ashani *et al.*, 2016). Evolving PTE variants with such catalytic efficiencies toward V-agents involves several challenges: First, the catalytic efficiency of wild type PTE with V-type nerve agents (i.e. 0.07–1 × 10^4 M^{-1} min^{-1}) is 3–4 orders of magnitude lower than necessary. Second, the P–S bond of V-agents is inherently more difficult to hydrolyze than P–O bonds commonly found in OPs; the thio effect (Ashani *et al.*, 2013). Third, wild-type PTE preferentially hydrolyzes the less toxic R_P isomers of V-agents. Finally, a useful countermeasure should target the entire spectrum of chemical warfare nerve agent (CWNAs) and be stable for usage and long-term storage. Thus, ideally, an evolved PTE variant would efficiently hydrolyze VX, Russian VX (RVX) and Chinese VX (CVX) as well as G-type nerve agents (Tabun, Sarin, Soman and Cyclosarin).

Previously, we evolved recombinant mammalian serum paraoxonase 1 (PON1) and a bacterial PTE to detoxify G- and V-type agents (Gupta *et al.*, 2011; Goldsmith *et al.*, 2012; Cherny *et al.*, 2013). The resulting variants were shown to provide effective protection from lethal nerve agent doses *in vivo* (Worek *et al.*, 2014a, b; Wille *et al.*, 2016). However, the catalytic efficiencies we obtained with V-type nerve agents would have required high enzyme doses to confer effective protection from VX in humans. We therefore aimed to further improve the most effective V-type degrading PTE variants we obtained so far, C23 and A53 (Cherny *et al.*, 2013), by ≥10-fold with VX and by ≥15-fold with RVX to obtain k_{cat}/K_M values of ≥5×10^7 M^{-1} min^{-1} with both these agents.

Here, we summarize our efforts and describe the challenges associated with overcoming the optimization plateau we encountered during the directed evolution of PTE. We discuss specific obstacles on the pathway to catalytic efficiency optimization, such as the tradeoff in activity between the two target substrates, VX and RVX, and the loss of stability that accompanied the acquisition of mutations. Overall, eight additional rounds of library generation and screening, including significant stabilization of the evolving enzyme were required to obtain PTE variants with the desired catalytic efficiencies. The evolved variants were also found to be highly efficient at detoxifying G-type nerve agents, especially Tabun (GA) and Sarin (GB). Thus, a combination of two or three evolved PTE variants that differ by only a few mutations may provide broad-spectrum nerve agent prophylaxis, and post-exposure V-agent treatment, using relatively low enzyme doses.

Results

Optimization of V-agent hydrolyzing PTE variants

Our starting point in this work, PTE variant C23, was the end point of our previous directed evolution effort to improve PTE's efficiency of V-agent hydrolysis (Cherny *et al.*, 2013). C23 was the outcome of five rounds of directed evolution, whereby a round consisted of the following steps: generation of a gene library from the best variants of the previous round, a screen for variants with higher detoxifying rates, isolation and verification of improved variants, and finally, purification and determination of catalytic efficiencies of improved variants. C23's catalytic efficiency was 5×10^6 M^{-1} min^{-1} with S_P-VX, and 0.7×10^6 M^{-1} min^{-1} with S_P-RVX (Table I).

To further increase the catalytic efficiency of C23 with V-agents, we used a previously developed screen that measures the ability of enzyme variants to prevent the inhibition of acetylcholinesterase (AChE) by OPs such as VX or RVX (Goldsmith *et al.*, 2012) (Fig. 1). In this screen, inactive PTE variants resulted in complete inhibition of AChE activity, while sufficiently active variants could hydrolyze the nerve agent before it inhibited AChE. Thus, the level of residual AChE activity correlated with the efficiency of the detoxifying PTE variant. V-agents were synthesized *in situ* as racemates (at non-hazardeous concentrations and amounts). However, since the S_P isomers of both VX and RVX inactivate hAChE at rates that are ~100-fold higher than those of the R_P isomers (Ordentlich *et al.*, 2004), the hydrolysis of the S_P isomer was the one primarily assayed.

Specifically, in each round one or more gene libraries of PTE were generated and cloned into an expression vector, transformed to *Escherichia coli* cells, and the transformed bacteria were grown on agar plates. Individual colonies were randomly picked, grown, and expressed in 96-deep well plates. The cultured cells were collected, lysed and combined with purified human AChE followed by VX and RVX. After a period of incubation, the residual AChE activity of the reaction mixture was measured (Materials and Methods, Fig. 1). The stringency of the screen was tuned at each round by altering the concentrations of the V-agents used, allowing us to assay for variants with increasingly higher detoxification rates. Subsequently the molar ratio of AChE to V-agents ranged from 1:10 up to 1:800 in the final rounds. The concentrations of the PTE variants in the lysates were in the same range as the AChE (~1 nM) although they were not directly screened for.

Table I. Catalytic efficiencies of hydrolysis of S_p-VX and S_p-RVX. (k_{cat}/K_M) $\times 10^6$ M^{-1} min^{-1} ± SD

Round #[a]	Variant	Mutational composition[b]	S_p-VX[c]	S_p-RVX[c]
0	PTE-S5[d]	–	0.01 ± 0.003 (**1**)	$7\times10^{-4} \pm 1\times10^{-4}$ (**1**)
5	C23[d]	K77A, A80V, F132E, T173N, G208D, H254G, I274N	5 ± 0.5 (**500**)	0.7 ± 0.02 (**1000**)
6	IVH3	K77A, A80V, I106A, F132E, T173N, G208D, H254G, A270E	2.8 ± 0.2 (**280**)	ND
7	IIIA3	K77A, A80V, I106A, F132E, T173N, G208D, D233N, H254G, S267M, I274N	3.7 ± 1 (**370**)	ND
8	82B5	C59F, K77A, A80V, I106A, S111R F132E, A203D, G208D, D233N, H254G, A270E, I274N	3.7 ± 1 (**370**)	ND
10	C23-Y309W	K77A, A80V, F132E, T173N, G208D, H254G, I274N, Y309W	7 ± 0.3 (**700**)	0.8 ± 0.02 (**1143**)
11	d1-C23-Y309W	K77A, A80V, F132E, T173N, G208D, H254G, I274N, Y309W, *R118E, A203D, S222D, S238D, M293V, G348T, T352E*	15 ± 1.0 (**1500**)	1.4 ± 0.20 (**2000**)
11	4E11	K77A, A80V, F132E, T173N, G208D, H254G, S267M, A270S, L271W, I274N, Y309W, *R118E, A203D, S222D, S238D, M293V, G348T, T352E*	31 ± 3.3 (**3100**)	0.4 ± 0.03 (**571**)
12	d1-IVA1	C59M, K77A, A80V, I106A, F132E, T173N, G208D, D233G, H254G, A266Del, I274N, Y309W, *R118E, A203D, S222D, S238D, M293V, G348T, T352E*	3.5 ± 0.8 (**350**)	12 ± 1.30 (**17 143**)
13	1-3-D5	K77A, A80V, F132E, T173N, G208D, D233G, H254G, I274N, Y309W, *R118E, A203D, S222D, S238D, M293V, G348T, T352E*	28 ± 3.0 (**2800**)	2.5 ± 0.20 (**3571**)
13[e]	1-3-D5 I106C	K77A, A80V, I106C, F132E, T173N, G208D, D233G, H254G, I274N, Y309W, *R118E, A203D, S222D, S238D, M293V, G348T, T352E*	6 ± 0.7 (**600**)	1.4 ± 0.50 (**2000**)
13[e]	1-3-D5 I106A	K77A, A80V, I106A, F132E, T173N, G208D, D233G, H254G, I274N, Y309W, *R118E, A203D, S222D, S238D, M293V, G348T, T352E*	23 ± 0.1 (**2300**)	6.3 ± 0.80 (**9000**)
13	10-2-C3	K77A, A80M, F132E, T173N, G208D, D233G, H254G, A270S, L271W, I274N, Y309W, *R118E, A203D, S222D, S238D, M293V, G348T, T352E*	50 ± 5.0 (**5000**)	3.2 ± 0.01 (**4571**)
13[e]	10-2-C3-I106C	K77A, A80M, I106C, F132E, T173N, G208D, D233G, H254G, A270S, L271W, I274N, Y309W, *R118E, A203D, S222D, S238D, M293V, G348T, T352E*	7 ± 1.0 (**700**)	1.2 ± 0.10 (**1714**)
13[e]	10-2-C3-I106A	K77A, A80M, I106A, F132E, T173N, G208D, D233G, H254G, A270S, L271W, I274N, Y309W, *R118E, A203D, S222D, S238D, M293V, G348T, T352E*	7 ± 0.2 (**700**)	8.3 ± 1.10 (**11 857**)
13	10-1-D11	K77A, A80M, F132E, T173N, G208D, D233G, H254G, S267M, A270S, L271W, I274N, Y309W, *R118E, A203D, S222D, S238D, M293V, G348T, T352E*	51 ± 8.0 (**5100**)	2.7 ± 1.10 (**3857**)
13[e]	10-1-D11-I106C	K77A, A80M, I106C, F132E, T173N, G208D, D233G, H254G, S267M, A270S, L271W, I274N, Y309W, *R118E, A203D, S222D, S238D, M293V, G348T, T352E*	11.5 ± 0.1 (**1150**)	1.5 ± 0.20 (**2143**)
13[e]	10-1-D11-I106A	K77A, A80M, I106A, F132E, T173N, G208D, D233G, H254G, S267M, A270S, L271W, I274N, Y309W, *R118E, A203D, S222D, S238D, M293V, G348T, T352E*	8 ± 0.4 (**800**)	10 ± 2.40 (**14 286**)

[a]Round #0 indicates the wt-like variant PTE S5 (Roodveldt and Tawfik, 2005). Rounds #1–4 were described in (Cherny *et al.*, 2013). No improved variant was isolated from Round #9.

[b]Substitutions relative to wt-like PTE S5. Computationally designed stabilizing mutations indicated in italics.

[c]In brackets—fold improvement relative to wt. like PTE S5 (Roodveldt and Tawfik, 2005). ND—not determined.

[d]Data taken from (Cherny *et al.*, 2013).

[e]Rationally constructed variants.

Following each round, clones that exhibited ≥2-fold residual AChE activity relative to the best variants from the previous round were isolated and retested. In this verification screen, three to six subclones of the initially isolated variants were grown and re-screened for AChE protection in order to eliminate false positives. Reproducibly improved clones were then purified and their catalytic efficiencies with VX and RVX were determined. The best variants from each round were then used as the starting point for the generation of the successive gene library.

The strategies used for making the libraries, and the results of each round are summarized in Tables II and III. Described below is a brief, retrospective narrative of the directed evolution trajectory.

Reaching the improvement plateau

Initially, we examined additional variants from a previously screened round #5 library (Cherny *et al.*, 2013). Aiming to increase library coverage, we screened 900 randomly selected variants using either VX or RVX. We identified variants improved with RVX but not with VX. The genes encoding the eight most improved RVX clones were shuffled to generate library 6-1 (Supplementary Table S1). In parallel, we designed library 6-2, in which two active-site residues (i.e. positions 270, 273; amino acid numbering follows PDB 1HZY), were selectively mutated on the background of C23 and two other variants described by Cherny *et al.* (A53 and G23; Supplementary Table S2). These two positions were chosen based on a computational model of

the complex of C23 with the transition state of VX (based on C23's crystal structure; Dym *et al.*, in preparation). This model suggested that these two residues are in contact with the substrate, and mutations may therefore improve VX binding. Round 6 libraries were screened using a mixture of VX and RVX in order to select for broad-spectrum variants that could efficiently hydrolyze both substrates. The six best variants of both libraries (6-1, 6-2) were purified and showed improvement of ~2-fold, yet again only with RVX.

Library 7-1 (Supplementary Table S3) was designed to examine substitutions at position 271 only, on the background of variants A53 and G23, while library 7-2 introduced rationally, and Rosetta-designed mutations (see Materials and Methods). Library 7-2 was generated on the background of a shuffled mixture of the genes encoding the best variants from round 6 (Supplementary Table S4). Following the failure of the previous rounds to identify variants with improved VX detoxification rates, the libraries were separately screened with VX and RVX. However, no improved clones were found after screening library 7-1 with VX or with RVX, and initially isolated clones from library 7-2 were later shown to have only minor improvements (<2-fold increases in rates of RVX neutralization relative to A53, and no improvement compared to C23 in VX) in the verification screen.

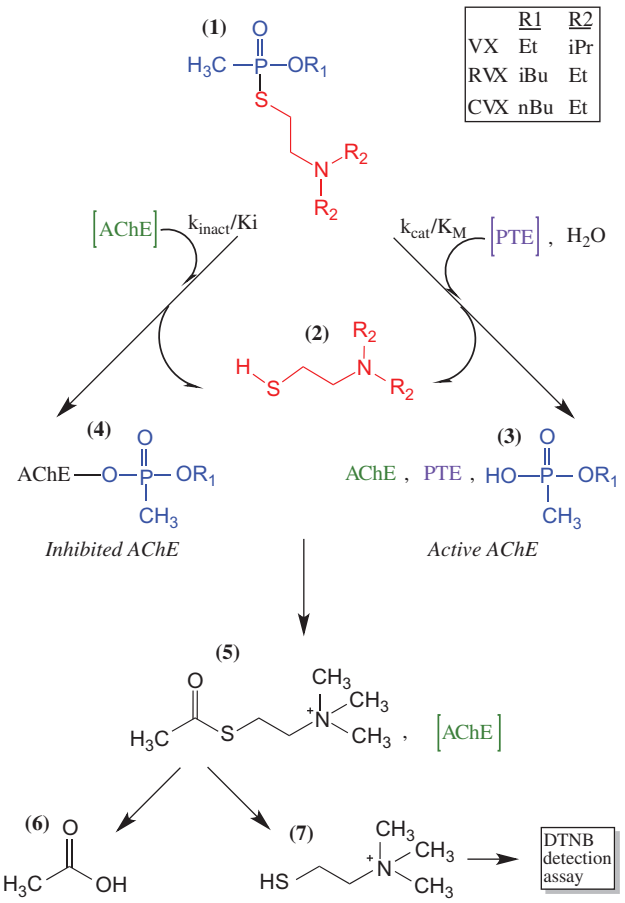

Fig. 1 A Scheme of the screening assay. (1) V-type nerve agents react either with acetylcholinesterase (AChE) to give the covalently inhibited enzyme (4; left arrow) or may be hydrolyzed by PTE (3; right arrow). The uninhibited AChE hydrolyzes the subsequently added substrate acetylthiocholine (5), thereby releasing thio-acetylcholine (7) that is detected by a reaction with DTNB; 5,5-Dithiobis (2-nitrobenzoic acid).

Round 8 (Supplementary Tables S5–S8) explored substitutions in positions in which beneficial mutations occurred in the earliest rounds leading to variant C23. In our previous work (Cherny *et al.*, 2013), two key beneficial mutations of C23, H254G and F132E, were selected. The rationale for revisiting these positions was as follows: Position 254 tolerated multiple amino acid substitutions in the first round, but the mutation H254G dominated the best variants of the second round. The mutation F132E was introduced following computational modeling using Rosetta, and was also selected in the second round. However, key adaptive mutations often interact with negative epistasis; i.e. they may be beneficial on their own but deleterious when combined with other mutations (Dellus-Gur *et al.*, 2015). Hence, shifting evolutionary trajectories may demand, e.g. reversion to wild-type sequence in one adaptive position in order to enable a second adaptive mutation to open a new trajectory (Salverda *et al.*, 2011). To explore reversion as well as alternative options, round 8 (library 8-3) targeted mutations to position 132 including reversion to the wild type amino acid, Phe (Supplementary Table. S7). In parallel, library 8-4 targeted position 254, including reversion to an Asn, a previously found beneficial mutation (Supplementary Table. S8). However, none of these substitutions improved activity (including E132F, the wild-type residue). In fact, substitution of E132 to Asp (a previously beneficial mutation) resulted in a 2-fold loss of VX hydrolysis activity and a 2 to 6-fold reduction in RVX hydrolysis. These results indicated that E132 not only plays a key role in evolved variants, but that it is also positively interacts with other positions. Whilst we cannot exclude the existence of alternative trajectories, these results suggest that if such trajectory(s) exist they differ fundamentally from the trajectory that had been followed.

The successive rounds, 9 to 10-2 (Supplementary Tables S9–S11), also failed to yield improved variants both in rationally and computationally designed libraries. Small improvements (~2-fold in VX) were only observed in individually constructed variants that carried rationally designed single point mutations (Library 10-3, Supplementary Table S11). At this point, we concluded that we had reached a plateau in the improvement of catalytic efficiencies (rounds 5–10, Fig. 2).

Stabilization of the evolving PTE variants

Whether the optimization plateau we had reached with PTE was local or global was unclear. We suspected, however, that the accumulation of mutations (i.e. 9–12 per gene) in selected variants along 10 directed evolution rounds had considerably reduced their

Table II. Summary of library making strategies

Strategy	Description
I	Amino acid substitutions (typically ≥3 per site), targeted to one or more sites, applied to either single or multiple variants without shuffling; on average ~2 substitutions per library variant.
II	Shuffling of selected variants with or without the incorporation of new mutations.
III	Simultaneous mutagenesis of sets of positions (typically 4–6 per variant) using site-specific substitutions.
IV	Rationally designed site directed mutants with up to 3 mutations per variant.
V	Whole gene random mutagenesis

Table III. Summary of the directed evolution screening rounds

Round #	Library #	Library making strategy[a]	Template clones shuffled #	Positions targeted for mutagenesis #	Theoretical library diversity[b]	Clones screened #	Nerve agents[c]	Improved variants initially identified # (substrate)
5[d]	5	I	7	8	1260	900	VX, RVX	8 (VX+RVX), 5 (RVX), 6 (VX)
6	6-1	II	8	0	27 648	420	VX+RVX	5 (VX+RVX)
	6-2	I	3	2	2116	420	VX+RVX	9 (VX+RVX)
7	7-1	I	2[e]	1	13	168	VX, RVX	0
	7-2	II	12	9	2.48×10^8	670	VX, RVX	24 (VX, RVX)
8	8-1	I	7[e]	1	7	168	VX, RVX	7 (VX, RVX)
	8-2	I	5[e]	1	7	84	VX, RVX	11 (VX, RVX)
	8-3	I	8[e]	1	6	84	VX, RVX	12 (VX, RVX)
9	9-1	III	1[e]	5	75	336	VX	10 (VX)
	9-2	III	1[e]	5	96	336	VX	11 (VX)
	9-3	III	1[e]	4	180	336	VX	11 (VX)
	9-4	III	1[e]	6	2268	168	VX	9 (VX)
	9-5	III	1[e]	5	360	252	VX	20 (VX)
	9-6	I	1[e]	2	400	252	VX	10 (VX)
	9-7	IV	1[f]	7	13	13[g]	VX	7 (VX)
10	10-1	I	1[e]	6	5600	420	VX	13 (VX)
	10-2	I	1[e]	4	4096	420	VX	24 (VX)
	10-3	IV	1[e]	6	14	14[g]	VX	7 (VX)
11	11-1	IV	1[e]	3	120	440	VX	1 (VX)
	11-2	IV	3[e]	4	90	440	VX	0
12	–	I	1[e]	4	16	504	RVX	4 (RVX)
13	13-1	V	1[e]	336	ND[h]	1512	VX	2 (VX)
	13-2	I	1[e]	5	96	756	VX	9 (VX)

[a]Library making strategy—see Table II.

[b]Calculated by assuming gene diversity due to shuffling as well as spiked mutations. On average, two mutations were spiked per clone in most libraries.

[c]Nerve agents used for the screen were VX, RVX or a mixture of both (VX + RVX).

[d]Rounds 1–5, beginning with PTE-S5 were described in (Cherny *et al.*, 2013). Library 5 was created by (Cherny *et al.*, 2013) and re-screened here. Consecutive rounds described here are numbered 6–13.

[e]Not shuffled. Each clone mutated separately as a template.

[f]Fold improvement in cell lysates relative to C23 for VX and relative to A53 for RVX.

[g]Single-double or triple mutants made were individually purified and examined.

[h]ND—not defined.

stability. Loss of stability may result in a reduction in the level of active, soluble enzyme with nearly every additional mutation incorporated into the gene (Tokuriki and Tawfik, 2009; Sikosek and Chan, 2014). Thus, screens of mutant libraries of marginally stable variants are likely to fail to identify mutations that confer improvements, and especially small improvements. Indeed, the inactivation mid-point temperature (i.e. the temperature at which 50% of the enzymatic activity is lost) of the best variant from round 10 that incorporated nine mutations, C23-Y309W (46°C), was 6°C lower than that of the starting point PTE-S5 variant (52°C; Fig. 3a).

Enzyme instability is usually indicated by reduced levels of solubly expressed enzyme. Variations in expression levels between variants were observed in crude cell lysates, however, the differences were relatively small and not clearly correlated with specific activity (data not shown). The PTE variants in our screen were expressed in fusion with the maltose binding protein of *E. coli* (MBP, tagged at the N-terminus). MBP is known to exhibit chaperon-like properties lowering the tendency for misfolding and aggregation (Kapust and Waugh, 1999). It is therefore conceivable that some PTE mutants expressed in a soluble form yet were enzymatically impaired. This hypothesis was later supported by the higher specific activity of the stabilized variant, as discussed below.

Previously we introduced PTE-family consensus mutations (Lehmann *et al.*, 2000) derived from a sequence analysis, to boost PTE's stability while evolving it for higher activity. Three of these mutations (K77A, A80V and I274N) were incorporated into C23 (Cherny *et al.*, 2013). However, the potential for consensus stabilization is limited, especially in PTE that has only a few orthologues in the database, or can be exhausted with the accumulation of mutations. We therefore subjected PTE to a web-available protein stabilization algorithm, PROSS, which designs stabilizing mutations and increases soluble protein expression without impairing protein function (Goldenzweig *et al.*, 2016). Briefly, PROSS's workflow comprises three stages: (i) Homologous sequences of the target protein are analyzed and, for each position, the set of amino acids that appear frequently across the natural diversity of the protein family is derived. (ii) Starting from a high-resolution structure of the target protein (or of a close homolog), Rosetta computational design simulations (Whitehead *et al.*, 2012) identify the subset of individual mutations from the above set that are predicted to be independently stabilizing. (iii) Rosetta's combinatorial sequence design is used to identify the combinations of mutations from the above subset that lead to substantially improved native-state energy. The workflow also allows the exclusion of active-site and other known critical positions thus preserving the protein's function. To design C23 for higher stability we used the crystal structure of wild-type PTE as input (PDB 1HZY). Since the number of known sequences of PTE homologs is relatively low, we lowered the algorithm's minimal

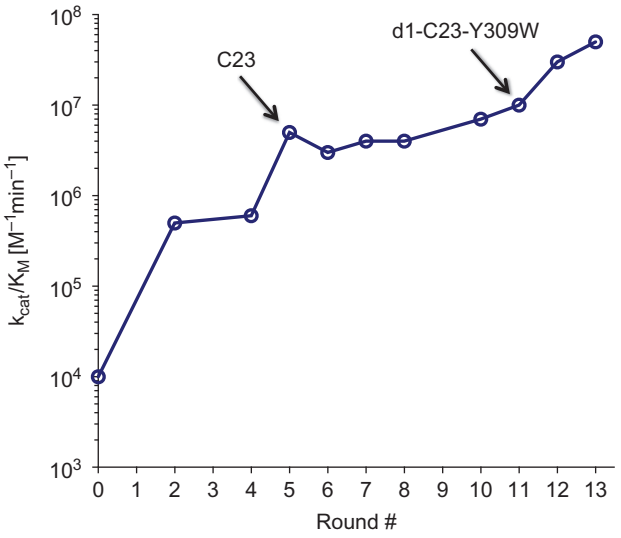

Fig. 2 The optimization of PTE's catalytic efficiency (k_{cat}/K_M) for hydrolysis of S_p-VX. The catalytic efficiency of the most active variant from each round of directed evolution is indicated. Round #0 denotes the wild-type-like variant PTE S5. Indicated are the names of two key variants on the graph: The starting point variant of this study, C23, obtained following five rounds of a previous directed evolution effort (Cherny *et al.*, 2013), and the stabilized variant di-C23-Y309W constructed in this work.

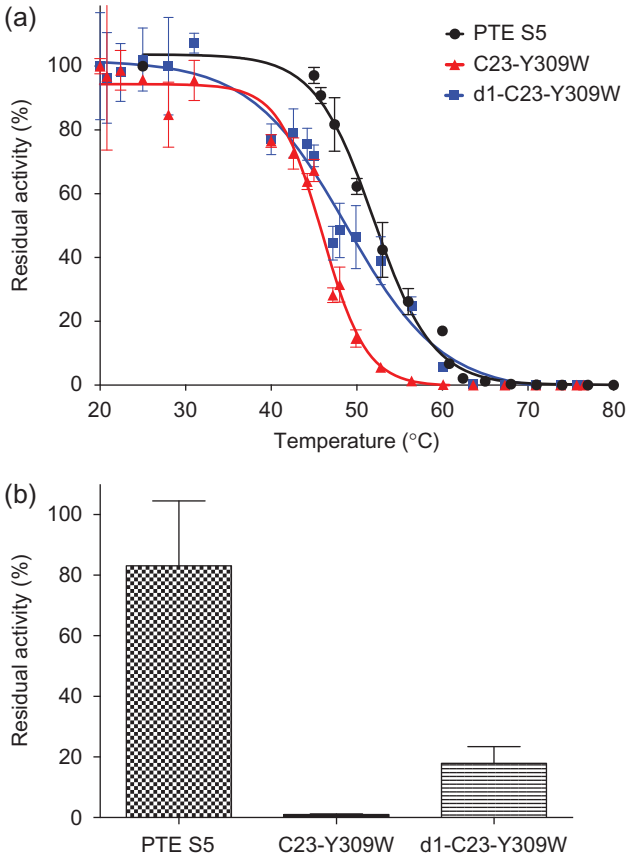

Fig. 3 Thermal stability and resistance to metal chelation of PTE variants. (**a**) Thermal inactivation assay. Purified wt-like PTE S5 (black line; ●), variant C23-Y309W (red line; ▲), and stabilized variant d1-C23-Y309W (blue line; ■), were incubated at different temperatures for 30 min in replicates (three per variant). The residual paraoxoanase activity was measured after cooling down to room temperature. Shown is the % residual activity (normalized to the activity of untreated enzyme) as a function of the incubation temperature. Data for purified PTE-S5 taken from (Goldenzweig *et al.*, 2016). (**b**) Metal-chelating inactivation assay. The purified proteins were incubated for 30 min at 37°C with 1,10-phenanthroline (50 μM). The residual paraoxonase activities are plotted relative to the protein activity in a zinc-containing buffer. Error bars denote the standard deviation ($n = 8$).

sequence identity threshold to include homologous sequences with ≥28% similarity. Amino acid positions at the active site and at PTE's dimeric interface were held fixed (see Materials and methods, Supplementary Table S12). Three designs were examined, bearing 7, 16 and 25 stabilizing mutations relative to C23 (and 9, 19 and 28 relative to PTE).

After testing these designs (Supplementary Figs S2, S3), we chose the best one, d1-C23-Y309W, which contained seven stabilizing mutations in addition to those of C23-Y309W and improved both in metal binding affinity and thermal stability (Fig. 3). The inactivation mid-point temperature of this variant was found to be 49°C (Fig. 3a), thus increasing the stability of the evolved variant C23-Y309W by 3°C. Notably, the activity of the stabilized variant (d1-C23-Y309W) with VX increased by 2-fold (Table I), although the stabilizing mutations were far from the protein's active site. This suggests that preparations of C23-Y309W contained soluble yet inactive, or poorly active enzyme. Such improvements in specific activity were seen in other PROSS stabilized enzymes (Goldenzweig *et al.*, 2016).

Further optimization of catalytic efficiency

In the next round, 11, we explored simultaneous substitutions of positions 267, 270 and 271 from loop 7, and of positions 303, 306, 309 and 310 from loop 8 (Supplementary Table S14). According to our docking models residues at these positions may be in contact with the substrate. However, since screening of libraries of individual mutations in these positions did not yield any improvements, we considered libraries of simultaneous substitutions. We also assumed that the stabilized background (d1-C23-Y309W) might enable acceptance of mutations that could not be previously accepted due to loss of stability. Our best variant from this round, 4E11, had three new mutations and was improved by 2-fold compared to d1-C23-Y309W ($k_{cat}/K_M = 3.1 \times 10^7\ M^{-1}\ min^{-1}$ with S_p–VX, Table I). Since the activity of this variant with VX was only 1.6-fold lower than our target goal, we aimed in the next round, 12, to optimize RVX hydrolysis activity. A detailed description of this round is presented in the next section. After we identified an improved RVX variant with a catalytic efficiency of ~$10^7\ M^{-1}\ min^{-1}$ with S_p–RVX in round 12, we continued to improve VX hydrolyzing activity in round 13.

Along the six rounds of directed evolution for VX hydrolysis described so far, and the five rounds previously described (Cherny *et al.*, 2013), we explored targeted substitutions at most of PTE's active-site positions. In some cases, we explored the same positions in different rounds. Overall, this strategy yielded significant improvements, but at this stage, it seemed to have been exhausted. Thus, we decided to generate variant libraries using whole-gene random mutagenesis. Screening ~1600 clones from a random mutagenesis library of stabilized variant d1-C23-Y309W (round 13-1), we identified two beneficial mutations, V80M and D233N. The first one, V80M, is probably a stabilizing mutation as it occurred in a position far from the active site, at which the stabilizing mutation (A80V) was previously identified (Tokuriki *et al.*, 2012; Cherny *et al.*, 2013).

However, D233N is an active site mutation that was actually found to be beneficial in earlier rounds (rounds 6–7, Supplementary Tables S1, S4a). We subsequently shuffled these two mutations (V80M and D233N) with the mutations of the best variant from round 11 (4E11) and with some rationally designed mutations (round 13-2; Supplementary Table S15). Screening the resulting round 13 library identified several variants that exhibited the desired catalytic efficiency toward VX ($k_{cat}/K_M = 5 \times 10^7\ M^{-1}\ min^{-1}$ with S_p-VX; Table I).

Engineering RVX hydrolyzing variants

The best previously evolved RVX hydrolyzing variant, A53, exhibited 5-fold higher catalytic efficiency for S_p-RVX hydrolysis than C23 (Cherny *et al.*, 2013). However, its k_{cat}/K_M value ($3.5 \times 10^6\ M^{-1}\ min^{-1}$) was >10-fold lower than our catalytic efficiency goal. A53 was also found to be unstable with a high tendency to misfold and aggregate. Initially, we attempted to evolve C23 both for VX and RVX hydrolysis. Accordingly, in rounds 5, 7 and 8 we screened separately with VX and RVX, and selected only variants that showed improved activity with both substrates. In round 6, we screened for detoxification of a mixture of both agents (Table III). The failure to identify improvements suggested a tradeoff between these two substrates. This tradeoff was somewhat unexpected because of the relatively small structural differences between VX and RVX (Supplementary Fig. S1) but became evident when individual variants were characterized. For example, the catalytic efficiency of our best round 11 variant, 4E11, with RVX was ~78-fold lower than it efficiency with VX (Fig. 4) and 125-fold lower than our goal (Table I). Nonetheless, upon analyzing selected variants from rounds 1 to 7, we identified one relatively efficient RVX hydrolyzing variant, IVA1 (Goldsmith *et al.*, 2015). Variant IVA1 had a catalytic efficiency of $5.3 \times 10^6\ M^{-1}\ min^{-1}$ with S_p-RVX and did not exhibit low stability as A53.

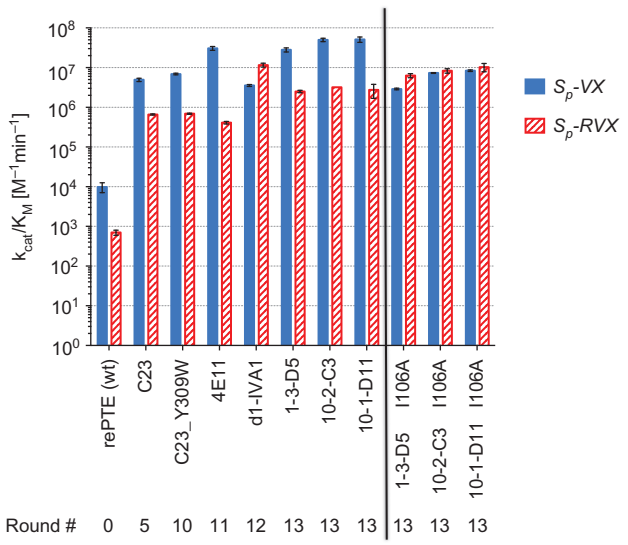

Fig. 4 Catalytic rate tradeoffs between VX and RVX. Plotted are the catalytic efficiencies (k_{cat}/K_M) of representative variants from different rounds of directed evolution with the S_p isomers of VX (blue bars) and RVX (red, stripped bars). The round number is presented at the bottom of the horizontal axis. Round 0 denotes the wt-like PTE-S5. Evolved variants are shown left to the vertical black line, and their engineered I106A mutants are shown to its right. Data for PTE-S5 and C23 are from (Cherny *et al.*, 2013).

In an attempt to increase the stability of this variant for further rounds of directed evolution, we grafted the mutations of IVA1 onto the stabilized design of d1-C23-Y309W. The resulting d1-IVA1 variant (Table I) also showed ~2-fold higher specific activity, as with d1-C23-Y309W described above, and a catalytic efficiency (k_{cat}/K_M) of $1.16 \times 10^7\ M^{-1}\ min^{-1}$ with S_p-RVX. Notably, despite the fact that the set of seven stabilizing mutations introduced into d1-C23-Y309W and d1-IVA1 was designed based the structure of wild-type PTE, and that both variants differ by up to 12 mutations from wild-type PTE, they were not only stabilized but also showed higher catalytic efficiency.

C23-Y309W and IVA1 differed in four positions (i.e. 59, 106, 233 and a deletion at position 266). We surmised, however, that one of these mutations is primarily responsible for the switch from VX to RVX. As previously noted (Cherny *et al.*, 2013; Goldsmith *et al.*, 2015), all variants that contained the I106A substitution exhibited more efficient hydrolysis of RVX than VX, and *vice versa*. Indeed, according to our computational model, position 106 is in direct contact with the *O*-alkyl groups of V-agents (Cherny *et al.*, 2013). We thus examined the effect of mutations of I106 to Ala or Cys, whose side chains length is intermediate, in the three most active VX hydrolyzing variants from the last round (round 13). As can be seen from Table I and Supplementary Fig. S4, mutating I106 to Cys decreased the rates with both RVX and VX. In contrast, mutating to Ala increased RVX activity by ~3-fold while decreasing the VX rates by ~7.5-fold. Since the initial VX/RVX activities ratio was on average 15 (Supplementary Fig. S4), the mutation of I106 to Ala resulted in variants that have almost equal detoxification efficiencies with VX and RVX (~$10^7\ M^{-1}\ min^{-1}$, Supplementary Fig. S5).

Evolved variants are broad-spectrum nerve agent detoxifiers

Although our priority had been to evolve optimized hydrolases of the more toxic nerve agents, VX and RVX, an applicable medical countermeasure should have broad-spectrum detoxification activity. As such, it should also promote the hydrolysis of the less toxic R_p isomers of VX and RVX, the S_p isomer of the less abundant threat agent Chinese VX (CVX), and also of G-type nerve agents (Supplementary Fig. S1). The large differences in the physicochemical properties of these agents make it unlikely that a single variant would efficiently hydrolyze all of them including their different isomers. A more likely scenario is that a mixture of a few variants that differ by only a small number of mutations would be able to provide broad-spectrum prophylactic activity against nerve agents. We thus examined the activity of our evolved variants with CVX, the R_p-isomers of V-agents and with G-type nerve-agents (Table IV).

The second-order rate constant for inhibition of hAChE by the S_p isomer of VX ($k_i = 1.4 \times 10^8\ M^{-1}\ min^{-1}$) is ~120-fold greater than that of its R_p isomer (Ordentlich *et al.*, 2004). Thus, it is sufficient for a catalytic bioscavenger to have an efficiency (k_{cat}/K_M), i.e. $\geq 5 \times 10^5\ M^{-1}\ min^{-1}$ with the R_p isomer of VX, in order to detoxify this isomer in the circulation before it inhibits blood cholinesterase activity. Our most active variants hydrolyze the R_p isomers of V-agents with k_{cat}/K_M values of $\geq 5 \times 10^5\ M^{-1}\ min^{-1}$ and thus amply meet this threshold (Table IV).

CVX is similar in structure to RVX except for its *O*-alkyl group (Supplementary Fig. S1). A previous analysis of selected variants from rounds 1–7 indicated that the toxic S_p isomers of CVX and RVX were hydrolyzed at very similar rates (Goldsmith *et al.*, 2015).

Table IV. Catalytic efficiencies of hydrolysis of nerve agents. k_{cat}/K_M ($\times 10^6$ M^{-1} min^{-1} ± SD)

Round #	Variant name	S_p-VX	R_p-VX	S_p–RVX	R_p-RVX	CVX-fast[a]	CVX-slow[a]	GA	GB	GD-fast	GD-slow	GF
0	PTE S5[b]	0.01 ± 3×10^{-3}	6.8 × 10^{-3} ± 2×10^{-4}	7×10^{-4} ± 1×10^{-4}	0.02 ± 1×10^{-3}	2×10^{-3} ± 2×10^{-4}	ND[c]	690 ± 140	8.2 ± 0.7	1 ± 0.3	0.1 ± 0.03	0.05 ± 8 × 10^{-3}
5	C23[b]	5 ± 0.5	0.65 ± 7×10^{-3}	0.7 ± 0.02	3 ± 0.3	1.7 ± 0.2	ND[c]	158 ± 18	148 ± 24	8.3 ± 2.5	8.3 ± 2.5	4.6 ± 0.03
10	C23-Y309W	7 ± 0.3	0.80 ± 0.2	0.8 ± 0.02	5.90 ± 0.3	ND[c]	ND[c]	ND[c]	ND[c]	ND[c]	ND[c]	ND[c]
11	d1-C23-Y309W	15 ± 1.0	0.8 ± 0.1	1.4 ± 0.20	4.5 ± 0.8	7.5 ± 1.4	1.9 ± 0.8	ND[c]	ND[c]	ND[c]	ND[c]	ND[c]
11	4E11	31 ± 3.3	0.70 ± 0.1	0.4 ± 0.03	0.50 ± 0.1	1.10 ± 0.1	0.4 ± 0.03	ND[c]	ND[c]	5.1 ± 1.7	0.75 ± 0.01	3.5 ± 0.1
12	d1-IVA1	3.5 ± 0.8	0.5 ± 0.1	12 ± 1.30	4.6 ± 0.6	7.5 ± 1.4	1.9 ± 0.8	ND[c]	ND[c]	3.8 ± 0.04	1.1 ± 0.1	1.5 ± 0.1
13	1-3-D5	28 ± 3.0	N.D[c]	2.5 ± 0.20	ND[c]	ND[c]	ND[c]	ND[c]	64 ± 7	ND[c]	ND[c]	1 ± 0.2
13	10-2-C3	50 ± 5.0	2.5 ± 0.1	3.2 ± 0.01	0.9 ± 0.1	3.7 ± 0.2	1.8 ± 0.6	279 ± 49	83 ± 22	1.4 ± 0.1	0.2 ± 0.02	3 ± 0.6
13	10-1-D11	51 ± 8.0	2.0 ± 0.2	2.7 ± 1.10	0.7 ± 0.01	3.4 ± 0.01	1.1 ± 0.1	126 ± 80	55 ± 7.5	0.7 ± 0.1	0.7 ± 0.1	3.2 ± 1.1

[a]CVX was assayed as a racemic mixture and its isomers were identified only by their rate of hydrolysis.
[b]Taken from (Cherny *et al.*, 2013).
[c]ND—not determined.

Evolved variants from rounds 11–13, exhibited similar catalytic efficiencies with S_p-RVX and the rapidly hydrolyzed isomer of CVX (Tables I, IV). Although we did not resolve the identity of the hydrolyzed CVX isomers, the structural similarity to RVX suggests that the rapidly hydrolyzed isomer is S_p-CVX. Thus, our most improved RVX hydrolyzing variant, d1-IVA1, may also provide effective protection from CVX.

Previously, we found that some G-agents such as GA and GB were efficiently hydrolyzed by PTE variants that were evolved toward VX (Cherny *et al.*, 2013). Here, we tested for the ability of our evolved variants to hydrolyze all G-type nerve agents and found that they hydrolyze the toxic isomers of GF and GD with ~10–200-fold lower rates than V-agents (Table IV). GA and GB, on the other hand, were hydrolyzed at rates that far exceed our catalytic efficiency goal (5.5–28 × 10^7 M^{-1} min^{-1}, Table IV).

The origins of catalytic improvements

PTE has evolved to hydrolyze the pesticide parathion and its oxidation product, paraoxon (Supplementary Fig. S1) with very high catalytic efficiency ($k_{cat}/K_M \approx 10^9$ M^{-1} min^{-1}) (Dumas *et al.*, 1989). Paraoxon differs from V-type nerve agents in several aspects: (i) Unlike V-agents, paraoxon does not have a chiral phosphorous center. (ii) Paraoxon is a phosphotriester with two *O*-ethyl substituting groups while V-agents are phosphonates with one *O*-alkyl substituting group. (ii) The pK_a of the phenol leaving-group of paraoxon is 7.15 (Serjeant and Dempsey, 1979) while that of V-agents is 7.9 (Maglothin and Wilson, 1974). (iv) Foremost, hydrolysis of paraoxon requires a P–O bond cleavage while that of V-agents involves a P–S bond cleavage. PTE exhibits a large thio-effect; i.e. the rate of thio-phosphoester hydrolysis by PTE is ~10^3-fold compared to an oxo-phosphoester with the same pK_a (Hong and Raushel, 1996; Ashani *et al.*, 2013).

Given these differences, the large increase in the efficiency of VX hydrolysis by evolved PTE variants was expected to result in a concomitant decrease in the catalytic efficiency of paraoxon hydrolysis. However, in agreement with previous observations (Khersonsky and Tawfik, 2010), we found a weak tradeoff between the two activities. Although the evolved variants improved by up to 5000-fold in VX hydrolysis (e.g. 4E11, 10-1-D11 compared to wild-type PTE; Table I) their paraoxonase activity was reduced by only 26-fold (Supplementary Table S16). A significantly larger decrease in catalytic efficiency for paraoxon was found in variants that contained the I106A substitution (i.e. up to 387-fold; Supplementary Table S16). This difference supports the role of position 106 in binding the *O*-alkyl group of the substrate and aligning it for catalysis. Finally, we observed similar rate decreases with paraoxon and parathiol, the P–S ester analog of paraoxon (and also with parathion, the P = S analog; Supplementary Fig. S1, Table S16). This result indicated that there was no selective improvement in the ability of the evolved variants to breakdown a P–S bond compared to a P–O bond.

In light of the above, we suggest that the mutations incorporated into PTE along this directed evolution trajectory did not increase its catalytic efficiency by modifying its catalytic mechanism. Rather, these mutations improved the alignment of V-agents in PTE's active site such that the frequency of catalytically productive substrate binding events increased. An increase in catalytic efficiency can result from a reduction in K_M, an increase in k_{cat} or both. Increased turnover rates (k_{cat}) can result from a larger fraction of substrate binding events that lead to product formation rather than dissociation (Bar-Even *et al.*, 2015). Unfortunately, due to toxicity and

solubility limitations, we were unable to measure individual K_M and k_{cat} values for the V-agents.

Discussion

Directed evolution can be viewed as an experimental algorithm applied to bypass knowledge gaps in our understanding of protein sequence, structure and function relations. It seems to work rather well for moderate increases in weak, promiscuous enzymatic activities. However, success is less obvious in deriving variants whose selected traits (e.g. substrate selectivity and catalytic efficiency) are several orders of magnitude greater than that of the starting point enzyme. Simply performing more rounds of mutagenesis and screening or selection does not guarantee that the target goals will be achieved. Prolonged directed evolution efforts are likely to result in 'diminishing returns' in which the magnitude of improvements in the selected trait decreases with every round of mutagenesis and selection. An inevitable outcome of strong diminishing returns is an 'optimization plateau', whereby library screens fail to identify variants with further improved catalytic efficiency.

Diminishing returns and optimization plateau

We aimed to further improve the catalytic efficiency of a previously described V-agent hydrolyzing PTE variant, C23, by 10-fold with S_p–VX and by 76-fold with R_p–RVX. These improvements seemed modest in comparison to the 525- and 943-fold increases in VX and RVX hydrolytic activity obtained by C23 within 5 rounds of directed evolution (Cherny *et al.*, 2013). However, following 5 additional rounds of directed evolution, our best variant (C23-Y309W, obtained in round 10) was improved only by 0.4-fold over C23 with VX, and not improved for RVX at all (Table I). In fact, none of the 5500 random clones screened from the 18 different libraries we constructed had shown any significant improvement in VX hydrolysis. The best clone from round 10 (C23-Y309W) was actually obtained by testing rationally designed single point mutants.

Like many other optimization processes, evolutionary optimizations are subject to diminishing returns. For example, a long directed evolution trajectory of PTE toward aryl esterase activity led to ~3×10^4-fold increase in catalytic efficiency upon 18 rounds of random mutagenesis and screening (Tokuriki *et al.*, 2012). However, the last round of that evolution gave 25-fold lower fold-improvement per mutation compared to the first one. In natural adaptive evolution, a similar phenomenon has been described in single genes (Schenk *et al.*, 2013), viruses (Rokyta *et al.*, 2011), unicellular organisms (Chou *et al.*, 2011) and multicellular organisms (Schoustra *et al.*, 2016).

Diminishing returns are therefore expected, thus making optimization plateaus inevitable. Upon encountering such a situation, the complexity of protein fitness landscapes burdens decision making. The experimentalist is faced with a number of difficult questions: can the 'plateauing' improvement rate of the evolved enzymatic activity be elevated? And if so, by how much more? Are there alternative evolutionary trajectories that can lead to higher activities (i.e. is this a local or global plateau)? Can the evolved enzyme 'cross-over' to these alternative trajectories? And if so, where is the crossing point? Adaptive mutations, typically the early ones, often interact with negative epistasis; i.e. they may be beneficial on their own but deleterious when combined (Dellus-Gur *et al.*, 2015) thus dictating discrete trajectories (Salverda *et al.*, 2011). Therefore, to access alternative trajectories, one might need to revert several mutations back to an early evolutionary intermediate or even to the starting point variant.

Orthogonal solution in PTE's sequence space

The fact that different sequence combinations, which can improve an enzyme toward a given substrate, may exist is also evident in the case of PTE and V-agents. Parallel efforts to enhance the catalytic efficiency of PTE with VX (Bigley *et al.*, 2013) and with RVX (Bigley *et al.*, 2015) have been described. The catalytic efficiency of the most efficient S_p-VX hydrolyzing variant of Bigley *et al.*, VRN-VQFL ($4.2 \times 10^6\ M^{-1}\ min^{-1}$) was similar to that of C23 ($5 \times 10^6\ M^{-1}\ min^{-1}$). However, these two variants have only two mutations in common (A80V, a stabilizing mutation, and I274N, an active-site mutation) and two substituted positions in common: 132 and 254 (Supplementary Table S17). The remaining five mutations in VRN-VQFL, and six in C23, were unique. In the case of RVX hydrolyzing PTE variants, the most catalytically efficient variant described by Bigley *et al.* (2015) was L7ep-3a I106G. Again, the sequence similarity to our variants was low: one identical substitution (I274N) and three shared positions (106, 132, and 254; Supplementary Table S18) for a variant with a similar catalytic efficiency.

We hypothesize that our mutational trajectory and the one followed by Bigley *et al.* are mutually exclusive. For example the amino acid occupying the key position 254 seems to dictate the occupancy at the key position 132 that resides on the opposite side of PTE's active site (Supplementary Fig. S6). Accordingly, in our evolutionary trajectory, the mutation F132E was only seen in variants that had Asn or Gly at position 254, but not in variants having Gln. Variants that had Gln at position 254 had Asp at 132 (Supplementary Table S2 in (Cherny *et al.*, 2013)). Accordingly, mutating 132 from Glu to Asp at advanced stages of our trajectory resulted in near-complete loss of VX activity. The variant QF (H254Q/H257F) was the starting point variant in the evolution of PTE for VX hydrolysis by Bigley *et al.* (2013). The next beneficial mutation was F132V and the combination F132V + H254Q became the core of all subsequently improved variants (Bigley *et al.*, 2013, 2015). Judging by the deleterious effect of the F132E + H254Q combination in our trajectory, the Bigley trajectory seems incompatible with our trajectory that was based on the F132E + H254G combination. Structural analysis may explain this incompatibility, although negative epistasis interactions between distal mutations may not be easy to detect (Dellus-Gur *et al.*, 2015). Whether the evolutionary trajectories pursued by Bigley *et al.* were exhausted (i.e. VRN-VQFL and L7ep-3a I106G comprise an optimization plateau), or whether they may lead to variants that are as active, or even more active than the ones described here is unknown. It is, however, clear that given sufficient library making and screening capacities, for example see (Obexer *et al.*, 2016), following several evolutionary trajectories in parallel during directed evolution may improve the chances of reaching the target goal.

Stabilization-enabled, continued evolutionary optimization

A hallmark of the 'diminishing returns' effect is the increasing identification of false-positive variants in advanced screening rounds. Such variants seemed improved when assayed in crude cell lysates, but not when assayed as purified proteins. The increased identification of false positives prompted us to examine whether protein stability began to dominate our screen for higher activity; i.e. that less active clones appeared to have a greater activity than clones that

were, in fact, more active, but expressed much lower levels of soluble, folded protein.

The marginal thermodynamic stability of most enzymes enables them to acquire only a few function-altering mutations (Bloom *et al.*, 2006; Tokuriki *et al.*, 2012). The computational stabilization of C23-Y309W improved not only its stability, but also increased its catalytic efficiency by twofold and boosted PTE's potential to evolve further. Up to four additional substitutions were successfully incorporated into the stabilized variant in just two successive rounds (rounds 12 and 13) thus increasing its VX activity. In fact, some of the newly acquired substitutions were included in libraries of previous rounds, yet were not selected (A270S in library 6-2, and S267M and D233G in library 7-2). Stabilization might have been a prerequisite for acquiring these beneficial mutations (Supplementary Tables S2, S4). An unexpected beneficial side effect of stabilization has been the increase of ~2-fold in catalytic efficiency of VX and RVX hydrolysis in stabilized variants. All the designed stabilizing mutations were of surface residues that reside in neither the active site nor the dimer interface. Accordingly, incorporation of these stabilized mutations increased activity irrespective of the composition of active-site mutations in evolved, marginally stable variants (VX-hydrolyzing C23-Y309W or RVX-hydrolyzing IVA1). Thus, the beneficial effect of these stabilizing mutations is exerted, in most likelihood, via an increase in the fraction of soluble and properly folded enzyme, and not by an influence on catalytic activity *per se*.

Overall, in our case, 'breaking away' from the improvement plateau' was enabled by the introduction of stabilizing mutations. A significant increase in stability was required and seven mutations, computationally designed, were simultaneously incorporated to achieve this task. The increase in stability therefore comprised a non-incremental move in sequence space. Some of these stabilizing mutations, or alternative ones, might have been individually predicted (e.g. by consensus analysis (Sullivan *et al.*, 2012), or specific algorithms (Bednar *et al.*, 2015; Magliery, 2015)), or selected by rounds of directed evolution for protein stability. However, their individual contribution to stability might have been difficult to detect, and the process of accumulating seven mutations would have been laborious and time consuming. The above said, protein stabilization might be a necessary condition for continued evolutionary optimization, but it is certainly not a sufficient one.

Activity tradeoffs lead to an optimization plateau

In retrospect, there were factors in addition to stability that seemed to have hindered our progress, foremost, activity tradeoffs. We attempted to simultaneously improve rates with both VX and RVX by selecting for variants that showed high activity with both substrates (rounds 5, 7 and 8), or even by using a mixture of both substrates in the screen (round 6). However, there seemed to be a strong tradeoff between these two substrates (Fig. 4). Thus, co-selection had probably hindered the identification of variants that were improved with one of the two substrates. The VX–RVX tradeoff also explains the unfortunate choice of staring point variants for the construction of some libraries. Sub-libraries 6-1 and 8-4, e.g. were designed on the basis of variants that did not contain the Ile at position 106 although I106 turned out to be crucial for activity with VX. The role of position 106 in switching the specificity of PTE between VX and RVX was recognized in our computational modeling (Cherny *et al.*, 2013) yet we assumed that there are mutational solutions that could provide high activity with both substrates. Apparently, we failed to identify such solutions. Thus, co-selection for two substrates, even if they differ slightly in their substituting moieties, as is the case for VX/RVX, may prevent the optimization of catalytic activity with either one.

Prospects for broad-spectrum nerve agent prophylaxis

V-type nerve agents are more toxic upon skin penetration, more stable and environmentally persistent than G-agents such as Sarin, Soman and Tabun (Munro, 1994). The limitations of currently available medical means for prevention and treatment of nerve agent intoxications in general, and of V-agents in particular, promoted the idea of using catalytic nerve-agent hydrolyzing enzymes as bioscavengers, in order to augment or replace current medical treatment protocols (Lenz *et al.*, 2007; Bird *et al.*, 2010; Worek *et al.*, 2016). The main advantage of using catalytic bioscavengers over non-catalytic ones, such as butyrylcholinesterase, is the ability to provide effective protection using a much lower enzyme-drug dose (Ashani and Pistinner, 2004) thus reducing both the cost and the risk of unwanted side-effects of bioscavengers (Schellekens, 2002). Highly efficient catalytic bioscavengers can also be used in decontamination and environmental bioremediation (Jacquet *et al.*, 2016).

Overall, following 13 rounds of directed evolution, the catalytic efficiency of PTE was improved up to 5.1×10^3-fold with VX and 1.7×10^4-fold with RVX. The evolved variants exhibit k_{cat}/K_M values that are 2–9-fold higher than the average natural enzyme, $6 \times 10^6\ min^{-1}\ M^{-1}$ although they are ~100-fold less efficient than wild-type PTE with its natural substrate paraoxon. According to our working model (Ashani *et al.*, 2016), the catalytic efficiencies obtained for all isomers of VX and RVX by our best variants (i.e. 10-2-C3 and 10-1-D11), in addition to their catalytic efficiencies with G-agents, and especially GA ($(13–28) \times 10^7\ min^{-1}\ M^{-1}$) and GB ($(6–8) \times 10^7\ min^{-1}\ M^{-1}$), suggest they can become advanced drug candidates for effective prophylaxis or post-exposure therapy of nerve-agent intoxication using low enzyme doses. These variants may also serve for non-corrosive, nerve-agent decontamination of personnel, equipment and surfaces.

Material and methods

PTE variant library construction

The PTE gene was cloned using EcoRI and PstI sites into a pMALc2x expression vector (NEB®) fused to an N-terminal MBP tag. Libraries of PTE variants were constructed using the following methods.

Site directed mutagenesis using single point mutations or degenerate codons (Table II, I, III, IV*)*: Single point mutations or degenerate NNK codons were encoded in the center of 22–28 bp synthetic oligonucleotides (oligo's). A reverse oligo encoding the complementary region was used for whole-plasmid PCR amplification using PfuUltra® II Fusion HS DNA Polymerase. The original plasmid was eliminated by digestion with DpnI (NEB®). The PCR product was purified using a PCR purification kit (QIAGEN®), phosphorylated using T4 PNK (NEB®) and 10 mM ATP (SIGMA) and ligated using T4 DNA ligase (Thermo®). Ligation products were purified by ethanol precipitation and transformed to electro-competent E.cloni® cells (Lucigen®). Cells were plated on LB-agar plates with Amp (100 mg/l). Plasmids containing the correct sequence were identified by colony PCR using Taq polymerase (Bio-ReadyMix®), isolated and transformed into the expression strain GG48 (Grass *et al.*, 2001) for screening.

Generating Targeted Libraries by the combinatorial incorporation of synthetic oligonucleotides during gene shuffling (Table II, II*)*: We

applied the ISOR method (Rockah-Shmuel *et al.*, 2014) as follows; amino-acid substitutions were introduced using short oligonucleotides encoding the mutated site flanked by the wild-type sequences. These were added to mixtures of 50–250 bp fragments of selected PTE variants, PCR amplified and cloned into a pMAL-c2x expression vector using EcoRI and PstI sites as described in (Rockah-Shmuel *et al.*, 2014). The protocol was tuned to obtain a combinatorial incorporation of the designed mutations at an average of 2 ± 1 mutations per gene.

Shuffled clones libraries (Table II, II*)*: Selected clones were PCR amplified using iPFU ready-mix (Intron®), DpnI digested and purified as described above. The PCR products were mixed at equal concentrations to a total of 20 µg DNA mix, digested to 50–250 bp fragments, purified and assembled to whole genes by PCR as described (Rockah-Shmuel *et al.*, 2014) without the introduction of spiking oligos. The PCR products were then cloned into the expression vector as described above.

Random mutagenesis libraries (Table II, V*)*: Whole-gene random mutagenesis was performed using the GeneMorph® II Random Mutagenesis Kit (Stratagene®) and oligos immediately upstream and downstream to MBP–PTE's ORF, using only 10 cycles and 0.5 µg template according to the manufacturer's protocol. The PCR product was then digested with DpnI, purified on Micro Bio-Spin™ 6 Columns (BioRad®), and amplified by PCR using iPFU ready-mix (Intron®). The resulting gene library was digested with EcoRI-HF® and PstI-HF® and cloned into a pMALc2x (NEB®) vector.

Computational library design

Initially, a transition state (TS) model was constructed with an in-line nucleophilic attack by a hydroxide on the phosphorus atom idealizing the TS geometry to a trigonal bipyramidal geometry (Aubert *et al.*, 2004). The TS models were superimposed onto the binuclear metal site of PTE variant C23 using the crystal structures with the phosphoryl oxygen coordinating the Znβ atom (Dym *et al.*, in preparation) and using the RosettaDock software suite (Meiler and Baker, 2006; Davis and Baker, 2009) to explore energetically favorable alignments. The top scoring docked poses were visually inspected and chosen for design and rigid body minimization. A distance restraint of 2.15 ± 0.25 Å was added between the phosphoryl oxygen and Znβ atom and a rigid-body minimization was performed using Talaris2014 (Leaver-Fay *et al.*, 2013) with RosettaScripts (Fleishman *et al.*, 2011). Interactions between models and enzyme were optimized using RosettaDesign algorithm (Kuhlman *et al.*, 2003). Substitutions were evaluated using a position-specific scoring matrix computed using psipred (McGuffin *et al.*, 2000) based on the PTE sequence from *Brevundimonas diminuta* followed by $\Delta\Delta G$ calculations using the $\Delta\Delta G$ monomer application (Kellogg *et al.*, 2011).

Computational design of stabilized C23 variants

To design stable variants of C23 we applied the PROSS algorithm (Goldenzweig *et al.*, 2016) on wild-type PTE, (pdb entry: 1HZY, chain A). To increase the diversity of homologs for the sequence analysis, we lowered the minimal sequence identity threshold to 28% (default is 30%). To avoid changes in the enzymatic function or disruption of PTE's active-site region all residues that are within 8 Å from the ligand *O*,*O*-diethyl-hydrogen-thiophosphate in PDB entry 4NP7 were selected (39 residues), assigned residue numbers as in pdb entry 1HZY, and excluded (i.e. held fixed in the Rosetta simulations). We also excluded 35 residues at PTE's dimeric interface (all residues within 5 Å from chain B). Three designs were selected for experimental testing; DNA sequences bearing the stabilizing mutations, the C23 mutations were ordered as synthetic DNA (Gen9®) with optimal codons for *E. coli* expression. The DNA was amplified by PCR using external primers and cloned into the expression vector pMALc2x using EcoRI and PstI restriction sites.

PTE library screening

Screening was performed essentially as described (Cherny *et al.*, 2013). Briefly, randomly picked colonies were individually grown O/N in 96-deep-well plates (Axygen®). Overnight cultures were used to inoculate (1:100 dilution) 0.5 ml LB medium with 100 µg/ml ampicillin and 0.1 mM $ZnCl_2$, grown to $OD_{600\ nm} \approx 0.6$, induced with 0.4 mM IPTG, and grown at R.T O/N. Cells were pelleted and lysed by resuspension and shaking in 300 µl/well of lysis buffer (0.1 M Tris pH 8.0, 0.1 M NaCl, 0.1% v/v Triton-X100, 0.2 mg/ml lysozyme, 10 mM Na_2CO_3 and 1:50 000 Benzonase nuclease). Lysates were centrifuged and kept at 4°C O/N before screening. Ovearll, 40 µl of clear cell lysate from each well were mixed with, 20 µl of *in situ* generated V-agents (50–4000 nM) and 40 µl of pure hAChE (human AChE, 2.5 nM). The reaction mixtures were incubated for 60 min before determination of residual AChE activity by mixing 20 µl of the reaction mixture with 180 µl PBS containing 0.85 mM DTNB and 0.55 mM acetylthiocholine. Initial velocities of acetylthiocholine hydrolysis were determined at 412 nm using a Powerwave HT spectrophotometer (BioTek®).

Enzyme expression and purification

The recombinant PTE variants (MBP N-terminal fusion) were expressed and purified as previously described (Cherny *et al.*, 2013). Briefly, the PTE genes were cloned into a pMALc2x expression vector (NEB®) and transformed into *E. coli* BL21/DE3 cells. The culture grew in 2 YT medium including ampicillin overnight at 37°C. The inoculate was dilute 1:100 into LB medium with ampicillin (100 µg/ml) and 0.2 mM $ZnCl_2$ and grown at 37°C to $OD_{600\ nm} \approx 0.6$. IPTG was added (0.4 mM), and the culture was allowed to grow overnight at 20°C. Cells were harvested by centrifugation and re-suspended in Lysis buffer (0.1 M Tris pH 8.0, 0.1 M NaCl, 10 mM $NaHCO_3$, 0.1 mM $ZnCl_2$, 0.4 mg/ml Lysozyme (Sigma®), 1:500 diluted protease inhibitor cocktail (Sigma®), 50 Units Benzonase nuclease (Merk®)). Cells were then lysed using sonication, clarified by centrifugation (10 000 × *g*, 4°C, 30 min) and passed through a column packed with amylose beads (NEB®) pre-equilibrated with 'wash buffer' (0.1 M Tris pH 8.0, 0.125 M NaCl, 10 mM $NaHCO_3$, 0.1 mM $ZnCl_2$). Following an extensive (10 c.v) wash using the 'wash buffer', the MBP–PTE fusion proteins were eluted with 'wash buffer' supplemented with 10 mM maltose. The fractions containing pure MBP–PTE variants were pooled and dialyzed overnight at 4°C with 0.1 M Tris pH 8.0, 0.1 M NaCl. Protein concentrations were examined by absorbance at 280 nm (extinction coefficient value for the MBP fused enzymes was $\varepsilon = 95925$ OD/M) and by PAGE-gel densitometry using BSA for calibration. Human AChE was cloned into the pHLsec expression vector (Aricescu *et al.*, 2006) and produced in large scale in HEK293T cells. The secreted protein was purified from the medium by affinity chromatography (Sussman *et al.*, 1988).

Enzyme kinetics

The hydrolysis rates of the individual isomers of VX or RVX and of racemic Chinese VX (CVX) were monitored by following the release of their thiol leaving groups using DTNB (Ellman *et al.*, 1961). To a

cuvette containing a 1 ml solution of 50 mM Tris–HCl (pH 8.0), 50 mM NaCl, and 0.7 mM DTNB (Ellman's reagent), we added purified PTE variants (final conc' range of 0.01 – 0.2 μM) and the mixture was pre-incubated at 25°C for 4 min. The hydrolysis reaction was initiated by the addition of V-agents (final concentration range of 10–30 μM). The increase in the concentration of thio-(2-nitro)-benzoic acid (Ellman's chromophore) in the reaction mixture as function of the reaction time was monitored continuously by measuring absorbance at 412 nm. Measurements were continued until ≥95% of the expected maximal absorbance was reached. The absorbance relating to 100% hydrolysis of the examined V-agent was determined separately by replacing the PTE solution with a solution of 0.5 M NaF in 50 mM phosphate buffer, pH 8.0. Data points were fitted to a mono exponential equation and the apparent first order rate constant was divided by the PTE concentration to obtain k_{cat}/K_M.

The detoxification rates of individual isomers of nerve agents were determined also using the AChE assay, essentially as described (Cherny *et al.*, 2013). Purified PTE variants (2.5–20 μl) were added to a buffered solution (1 ml, 50 mM Tris–HCl pH 8.0, 50 mM NaCl) containing 0.2–0.5 μM of the nerve-agent substrates. The final PTE concentration range was 1–200 nM. Solutions of individual nerve agent isomers (10–50 μM) were generated in water (details available upon request). At selected time intervals, aliquots (5–10 μl) were removed from the hydrolysis reaction into solutions of recombinant human AChE (0.2–0.5 ml, 10 mM phosphate buffer pH 8.0, final hAChE conc' 4–7 nM). The dilute aliquots were incubated for 60 min at RT to ensure complete interaction between the OPs and hAChE. Maximal hAChE inhibition was determined by dilution of the same OP concentration into the buffer solution (50 mM Tris–HCl pH 8.0, 50 mM NaCl) in the absence of the PTE variant, and kept at ≤90% by adjusting the OP concentration accordingly. Residual hAChE activity was determined by diluting the aliquot solution (50–100-fold) into a solution of acetylthiocholine iodide (ATC) (1 mM) and DTNB (0.7 mM) and monitoring absorbance at 412 nm over 1.5 min. The hAChE activity assay was repeated for each sample after 75–80 min to ascertain the percentage of hAChE inhibition. The spontaneous hydrolysis of ATC was subtracted from all ATC hydrolysis rates. The spontaneous hydrolysis of the nerve agents in 50 mM Tris, 50 mM NaCl pH 8.0 was negligible over the time period used to monitor detoxification by the PTE variants. The percentage of hAChE inhibition was calculated from the ratio of residual hAChE activity at each time point to the residual hAChE activity at $t = 0$ (before the addition of PTE). The apparent first-order detoxification rate constant (k) was obtained by fitting the plot of the % hAChE inhibition as a function of the incubation time to a single exponent. The catalytic efficiency k_{cat}/K_M was obtained by dividing k by the molar concentration of PTE.

Thermal inactivation assay

Samples of purified PTE proteins (20 μl, 0.5 μM) in 96-well PCR plates (Axygen®) were incubated in a gradient PCR (Biometra®) for 30 min at a range of temperatures, cooled to 4°C for 10 min, and moved to RT. The samples were diluted 1:10 in activity buffer (50 mM Tris–HCl pH 8.0, 50 mM NaCl) and their residual paraoxonase activity was measured by the addition of paraoxon (35 μM; total assay volume 200 μl). The OD_{405nm} was recorded for 5 min in a BioTek Synergy HT ELISA plate reader. Triplicate samples of each variant at each temperature were assayed. The residual activity was derived from the initial velocities of paraoxon hydrolysis for the heat-inactivated sample divided by the velocity observed for the untreated variant kept at room temperature. The inactivation mid-point temperature, i.e. the temperature leading to a residual activity of 50%, was calculated by fitting the residual activity at different temperatures to a 4-parameter Boltzmann sigmoidal curve: $A_t = A_0 + \frac{A_f - A_0}{1 + e^{(T_m - T)/m}}$; where A_t corresponds to the residual activity following incubation at a given temperature T, A_0 is the activity of the control sample at room temperature, A_f is the activity following incubation at the maximal inactivating temperature and m is the sigmoidal slope coefficient.

Metal chelation assay

Samples of purified PTE variants (20 μl, 0.5 μM) were transferred to 96-well PCR plates (Axygen®) and mixed either with a buffered solution (50 mM Tris–HCl pH 8.0, 50 mM NaCl) of 1,10-phenanthrolin (20 μl, 100 μM pH 8.0) or with a buffered solution of $ZnCl_2$ (20 μl, 10 μM pH 8.0). The plate was incubated for 30 min, either at room temperature (for the comparison of PROSS designs) or at 37°C (for the comparison made in Fig. 3b), and cooled to RT. The residual activity was determined as described above. Each variant was measured in eight replicates.

Supplementary data

Supplementary data are available at *Protein Engineering, Design & Selection* online.

Abbreviations

OP, organophosphate; AChE, acetylcholinesterase; PTE, phosphotriesterase; CWNA, chemical warfare nerve agent; VX; RVX, Russian VX.

Acknowledgments

D.S.T. is the Nella and Leon Benoziyo Professor of Biochemistry. Financial support by the Defense Threat Reduction Agency (DTRA) of the US Department of Defense (HDTRA1-11-C-0026) is gratefully acknowledged. The collaboration between the Fleishman and Tawfik laboratories is also supported by the Rothschild-Caesaria Foundation.

Funding

Financial support by the Defense Threat Reduction Agency (DTRA) of the US Department of Defense (HDTRA1-11-C-0026) and the Rothschild-Caesaria Foundation.

References

Althoff,E.A., Wang,L., Jiang,L., *et al.* (2012) *Protein Sci.*, **21**, 717–726. doi:10.1002/pro.2059.

Aricescu,A.R., Lu,W. and Jones,E.Y. (2006) *Acta Crystallogr. D Biol. Crystallogr.*, **62**, 1243–1250. doi:10.1107/S0907444906029799.

Ashani,Y., Goldsmith,M., Leader,H., Wieczorek,G., Silman,I., Sussman,J.L. and Tawfik,D.S. (2013) *FEBS J.*, **280**, 167–167.

Ashani,Y., Leader,H., Aggarwal,N., Silman,I., Worek,F., Sussman,J.L. and Goldsmith,M. (2016) *Chem. Biol. Interact.* doi:10.1016/j.cbi.2016.04.039.

Ashani,Y. and Pistinner,S. (2004) *Toxicol. Sci.*, **77**, 358–367.

Aubert,S.D., Li,Y. and Raushel,F.M. (2004) *Biochemistry*, **43**, 5707–5715. doi:10.1021/bi0497805.

Bar-Even,A., Milo,R., Noor,E. and Tawfik,D.S. (2015) *Biochemistry*, **54**, 4969–4977. doi:10.1021/acs.biochem.5b00621.

Bar-Even,A., Noor,E., Savir,Y., Liebermeister,W., Davidi,D., Tawfik,D.S. and Milo,R. (2011) *Biochemistry*, **50**, 4402–4410. doi:10.1021/bi2002289.

Bednar,D., Beerens,K., Sebestova,E., Bendl,J., Khare,S., Chaloupkova,R., Prokop,Z., Brezovsky,J., Baker,D. and Damborsky,J. (2015) *PLoS Comput. Biol.*, **11**, e1004556. doi:10.1371/journal.pcbi.1004556.

Benschop,H.P. and Dejong,L.P.A. (1988) *Acc. Chem. Res.*, **21**, 368–374.

Bigley,A.N., Mabanglo,M.F., Harvey,S.P. and Raushel,F.M. (2015) *Biochemistry*, **54**, 5502–5512. doi:10.1021/acs.biochem.5b00629.

Bigley,A.N., Xu,C.F., Henderson,T.J., Harvey,S.P. and Raushel,F.M. (2013) *J. Am. Chem. Soc.*, **135**, 10426–10432. doi: 10.1021/ja402832z.

Bird,S.B., Dawson,A. and Ollis,D. (2010) *Front. Biosci. (Schol. Ed.)*, **2**, 209–220.

Bloom,J.D., Labthavikul,S.T., Otey,C.R. and Arnold,F.H. (2006) *Proc. Natl. Acad. Sci. U.S.A.*, **103**, 5869–5874. doi:10.1073/pnas.0510098103.

Cherny,I., Greisen, P.Jr, Ashani,Y., Khare,S.D., Oberdorfer,G., Leader,H., Baker,D. and Tawfik,D.S. (2013) *ACS Chem. Biol.*, **8**, 2394–2403. doi:10.1021/cb4004892.

Chou,H.H., Chiu,H.C., Delaney,N.F., Segre,D. and Marx,C.J. (2011) *Science*, **332**, 1190–1192. doi:10.1126/science.1203799.

Currin,A., Swainston,N., Day,P.J. and Kell,D.B. (2015) *Chem. Soc. Rev.*, **44**, 1172–1239. doi:10.1039/C4CS00351A.

Davis,I.W. and Baker,D. (2009) *J. Mol. Biol.*, **385**, 381–392. doi:10.1016/j.jmb.2008.11.010.

Dellus-Gur,E., Elias,M., Caselli,E., Prati,F., Salverda,M.L., de Visser,J.A., Fraser,J.S. and Tawfik,D.S. (2015) *J. Mol. Biol.*, **427**, 2396–2409. doi:10.1016/j.jmb.2015.05.011.

Dumas,D.P., Caldwell,S.R., Wild,J.R. and Raushel,F.M. (1989) *J. Biol. Chem.*, **264**, 19659–19665.

Ellman,G.L., Courtney,K.D., Andres, V.Jr and Feather-Stone,R.M. (1961) *Biochem. Pharmacol.*, **7**, 88–95.

Fasan,R., Chen,M.M., Crook,N.C. and Arnold,F.H. (2007) *Angew. Chem. Int. Ed. Engl.*, **46**, 8414–8418. doi:10.1002/anie.200702616.

Fleishman,S.J., Leaver-Fay,A., Corn,J.E., *et al.* (2011) *PLoS One*, **6**, e20161. doi:10.1371/journal.pone.0020161.

Goldenzweig,A., Goldsmith,M., Hill,S.E., *et al.* (2016) *Mol. Cell*, **63**, 337–346. doi:10.1016/j.molcel.2016.06.012.

Goldsmith,M., Ashani,Y., Simo,Y., Ben-David,M., Leader,H., Silman,I., Sussman,J.L. and Tawfik,D.S. (2012) *Chem. Biol.*, **19**, 456–466. doi: 10.1016/j.chembiol.2012.01.017.

Goldsmith,M., Eckstein,S., Ashani,Y., *et al.* (2015) *Arch. Toxicol.* doi:10.1007/s00204-015-1626-2.

Grass,G., Fan,B., Rosen,B.P., Franke,S., Nies,D.H. and Rensing,C. (2001) *J. Bacteriol.*, **183**, 4664–4667. doi:10.1128/JB.183.15.4664-4667.2001.

Gupta,R.D., Goldsmith,M., Ashani,Y. *et al* (2011) *Nat. Chem. Biol.*, **7**, 120–125. doi: 10.1038/nchembio.510.

Hong,S.B. and Raushel,F.M. (1996) *Biochemistry*, **35**, 10904–10912. doi:10.1021/bi960663m.

Jacquet,P., Daude,D., Bzdrenga,J., Masson,P., Elias,M. and Chabriere,E. (2016) *Environ. Sci. Pollut. Res. Int.*, **23**, 8200–8218. doi:10.1007/s11356-016-6143-1.

Kapust,R.B. and Waugh,D.S. (1999) *Protein Sci.*, **8**, 1668–1674.

Kellogg,E.H., Leaver-Fay,A. and Baker,D. (2011) *Proteins*, **79**, 830–838. doi:10.1002/prot.22921.

Khare,S.D., Kipnis,Y., Greisen, P.Jr, *et al.* (2012) *Nat. Chem. Biol.*, **8**, 294–300. doi:10.1038/nchembio.777.

Khersonsky,O. and Tawfik,D.S. (2010) *Annu. Rev. Biochem.*, **79**, 471–505. doi:10.1146/annurev-biochem-030409–143718.

Kuhlman,B., Dantas,G., Ireton,G.C., Varani,G., Stoddard,B.L. and Baker,D. (2003) *Science*, **302**, 1364–1368. doi:10.1126/science.1089427.

Leaver-Fay,A., O'Meara,M.J., Tyka,M., *et al.* (2013) *Methods Enzymol.*, **523**, 109–143. doi:10.1016/B978-0-12-394292-0.00006-0.

Lehmann,M., Pasamontes,L., Lassen,S.F. and Wyss,M. (2000) *Biochim. Biophys. Acta*, **1543**, 408–415.

Lenz,D.E., Yeung,D., Smith,J.R., Sweeney,R.E., Lumley,L.A. and Cerasoli,D.M. (2007) *Toxicology*, **233**, 31–39.

MacLean,R.C., Perron,G.G. and Gardner,A. (2010) *Genetics*, **186**, 1345–1354. doi:10.1534/genetics.110.123083.

Magliery,T.J. (2015) *Curr. Opin. Struct. Biol.*, **33**, 161–168. doi:10.1016/j.sbi.2015.09.002.

Maglothin,J.A. and Wilson,I.B. (1974) *Biochemistry*, **13**, 3520–3527.

McGuffin,L.J., Bryson,K. and Jones,D.T. (2000) *Bioinformatics*, **16**, 404–405.

Meiler,J. and Baker,D. (2006) *Proteins*, **65**, 538–548. doi:10.1002/prot.21086.

Munro,N. (1994) *Environ. Health Perspect.*, **102**, 18–38.

Obexer,R., Pott,M., Zeymer,C., Griffiths,A.D. and Hilvert,D. (2016) *Protein Eng. Des. Sel.*, **29**, 355–366. doi:10.1093/protein/gzw032.

Ordentlich,A., Barak,D., Sod-Moriah,G., *et al.* (2004) *Biochemistry*, **43**, 11255–11265. doi:10.1021/bi0490946.

Rockah-Shmuel,L. and Tawfik,D.S. (2012) *Nucleic Acids Res.*, **40**, 11627–11637. doi:10.1093/nar/gks944.

Rockah-Shmuel,L., Tawfik,D.S. and Goldsmith,M. (2014) *Methods Mol. Biol.*, **1179**, 129–137. doi:10.1007/978-1-4939-1053-3_8.

Rokyta,D.R., Joyce,P., Caudle,S.B., Miller,C., Beisel,C.J. and Wichman,H.A. (2011) *PLoS Genet.*, **7**, e1002075. doi:10.1371/journal.pgen.1002075.

Roodveldt,C. and Tawfik,D.S. (2005) *Protein Eng. Des. Sel.*, **18**, 51–58. doi:10.1093/protein/gzi005.

Salverda,M.L., Dellus,E., Gorter,F.A., Debets,A.J., van der Oost,J., Hoekstra, R.F., Tawfik,D.S. and de Visser,J.A. (2011) *PLoS Genet.*, **7**, e1001321. doi:10.1371/journal.pgen.1001321.

Schellekens,H. (2002) *Clin. Ther.*, **24**, 1720–1740. discussion 1719.

Schenk,M.F., Szendro,I.G., Salverda,M.L., Krug,J. and de Visser,J.A. (2013) *Mol. Biol. Evol.*, **30**, 1779–1787. doi:10.1093/molbev/mst096.

Schoustra,S., Hwang,S., Krug,J. and de Visser,J.A. (2016) *Proc. Biol. Sci.*, **283**. doi:10.1098/rspb.2016.1376.

Serjeant,E.P. and Dempsey,B. (1979) *Ionisation Constants of Organic Acids in Aqueous Solution*. Pergamon Press, Oxford, New York.

Sikosek,T. and Chan,H.S. (2014) *J. R. Soc. Interface*, **11**. doi:10.1098/rsif.2014.0419.

Sullivan,B.J., Nguyen,T., Durani,V., Mathur,D., Rojas,S., Thomas,M., Syu,T. and Magliery,T.J. (2012) *J. Mol. Biol.*, **420**, 384–399. doi:10.1016/j.jmb.2012.04.025.

Sussman,J.L., Harel,M., Frolow,F., Varon,L., Toker,L., Futerman,A.H. and Silman,I. (1988) *J. Mol. Biol.*, **203**, 821–823.

Tokuriki,N., Jackson,C.J., Afriat-Jurnou,L., Wyganowski,K.T., Tang,R. and Tawfik,D.S. (2012) *Nat. Commun.*, **3**, 1257. doi:10.1038/ncomms2246.

Tokuriki,N. and Tawfik,D.S. (2009) *Curr. Opin. Struct. Biol.*, **19**, 596–604. doi:10.1016/j.sbi.2009.08.003.

Whitehead,T.A., Chevalier,A., Song,Y., *et al.* (2012) *Nat. Biotechnol.*, **30**, 543–548. doi:10.1038/nbt.2214.

Wijma,H.J. and Janssen,D.B. (2013) *FEBS J.*, **280**, 2948–2960. doi:10.1111/febs.12324.

Wille,T., Neumaier,K., Koller,M., *et al.* (2016) *Toxicol. Lett.*, **258**, 198–206. doi:10.1016/j.toxlet.2016.07.004.

Worek,F., Seeger,T., Goldsmith,M., Ashani,Y., Leader,H., Sussman,J.S., Tawfik,D., Thiermann,H. and Wille,T. (2014a) *Arch. Toxicol.*, **88**, 1257–1266. doi:10.1007/s00204-014-1204-z.

Worek,F., Seeger,T., Reiter,G., Goldsmith,M., Ashani,Y., Leader,H., Sussman,J.L., Aggarwal,N., Thiermann,H. and Tawfik,D.S. (2014b) *Toxicol. Lett.*, **231**, 45–54. doi:http://dx.doi.org/10.1016/j.toxlet.2014.09.003.

Worek,F., Thiermann,H. and Wille,T. (2016) *Toxicol. Lett.*, **244**, 143–148. doi:10.1016/j.toxlet.2015.07.012.

Yang,G. and Withers,S.G. (2009) *Chembiochem*, **10**, 2704–22715. doi:10.1002/cbic.200900384.

Zheng,F., Xue,L., Hou,S., Liu,J., Zhan,M., Yang,W. and Zhan,C.G. (2014) *Nat. Commun.*, **5**, 3457. doi:10.1038/ncomms4457.